BOLETIN DE LA SOCIEDAD ESPAÑOLA DE

Cerámica y Vidrio

A R T I C U L O

◆ ◆ ◆

Use of mud from metallic surface treatment industries as additive to ceramic matrices

F.A. CORPAS IGLESIAS[1], L. PÉREZ VILLAREJO[1], M. BENÍTEZ GUERRERO[2], R. ARTIAGA DÍAZ[3], J. PASCUAL COSP[2]

[1] Escuela Politécnica Superior de Linares, Universidad de Jaén, Linares, Jaén, Spain.
[2] Escuela Técnica Superior de Ingenieros Industriales, Universidad de Málaga, Málaga, Spain.
[3] Escola Politécnica Superior, Universidade da Coruña, Ferrol, A Coruña, Spain.

Ceramic processing is one of the most efficient and environmentally friendly solutions to the enormous amounts of industrial mud produced in metal surface treatments. Moreover, ceramized products may represent an important secondary source to replace clay materials and cut down manufacturing costs. After characterization, in order to prepare specimens by uniaxial die pressing, mud was incorporated into a clay matrix at rates between 1 and 5 wt %. Compression strength, linear contraction, suction capacity and water absorption of the moulded materials were evaluated. Finally, metal leakage was characterized through chemical analysis of lixiviates. The results showed an improvement in mechanical properties following the incorporation of mud into the ceramic materials. The resulting materials meet health and safety regulations regarding dangerous waste recycling.

Keywords: Valorization, Mud, Ceramic, Waste.

Lodos procedentes de la industria de tratamiento de superficies metálicas como aditivos a matrices cerámicas

La ceramización es una de las soluciones más eficientes y medioambientalmente más ecológicas para las enormes cantidades de lodos industriales que se producen en el tratamiento de superficies metálicas. Además estos lodos convenientemente ceramizados pueden representar una fuente de materia prima que sustituya en parte el consumo de arcilla, lo que se traduce en una disminución de los costes de fabricación. Tras caracterizarse, los lodos fueron incorporados en la matriz cerámica en proporciones desde el 1% hasta el 5%, fabricándose así piezas cerámicas por compresión uniaxial en seco. A las piezas conformadas se les midieron una serie de características tecnológicas tales como la resistencia a la compresión, la contracción lineal, capacidad de succión y la absorción de agua. Finalmente se realizaron análisis químicos de lixiviados para evaluar la liberación al medio de metales. Los resultados conseguidos muestran una mejora de las propiedades mecánicas tras la inclusión de los lodos en matrices cerámicas. Los materiales así fabricados satisfacen la normativa referente al reciclaje de residuos peligrosos.

Palabras clave: Valorización, Lodo, Cerámica, Residuo.

1. INTRODUCTION

One of the techniques employed to protect metals and alloys from corrosion is metal surface treatment. In this industrial process, huge amounts of water are consumed both in production and washing operations, with important amounts of industrial wastewater and mud being produced as a result [1, 2].

Anodized aluminium industry is an important sector where large quantities of industrial waste are generated. There is an ongoing effort to find ways to either recover some chemical species from industrial wastewaters and mud or treating them so that they can be used as raw materials in different processes [3].

The increasing environmental problems derived from the accumulation of industrial waste generated in metal surface treatment plants bring about the challenge of researching efficient and safe methods for treating, storing, and, eventually, finding new uses for these by-products. The social pressure stemming from environmental concerns, combined with the high costs of an adequate disposal of human activity waste reaffirms the need for a progressive reduction in waste volume. In this context, waste appreciation becomes even more important.

Building industry is particularly well suited to the purpose of assimilating huge amounts of solid industrial waste whether straight from production or after undergoing a transformation process [4,5]. One of the advantages of the building sector is that, besides absorbing enormous amounts of materials, it admits a broad range of qualities, which allows preparing a large range of materials according to standards for different applications. As several studies have shown, polymer, cement and ceramic based products are the most adequate materials for neutralization and inertization of waste by encapsulation in their matrix [6, 7, 8, 9].

Since clayey ceramics are made of clays with a broad range of compositions, they are very heterogeneous [10]. As

a result, these materials can admit different kinds of waste in important amounts [11], contributing to reduce building costs.

Among the existing techniques to inertize and neutralize industrial waste, ceramic processing is the most advantageous as far as output and cost are concerned, since the industrial waste coming from the surface treatment plants becomes chemically integrated within the ceramic material.

In order to obtain a good interaction between clay and waste, grain size should be as small as possible. A large grain size would lead to encapsulation instead of chemical interaction.

On the other hand, replacement of part of the clayey materials by industrial waste in traditional ceramic production can lead to important cost reductions in raw materials, as well as contribute to solving the stocking problems associated to this type of waste [12].

The aim of this work is to evaluate the potential use of industrial anodized aluminium mud waste in brick manufacturing.

2. MATERIALS AND METHODS

Two components were used for the preparation of ceramic materials: clay and industrial mud. The clay and the mud were provided by Arcillas Bailén S. L. (Bailén, Jaén) and Alusistemas S. L. (Mancha Real, Jaén) respectively. The clay was dried to constant weight at 110 ºC inside an electrical oven. It was then milled and sieved to 150 μm. The same drying process was applied to the mud. Next, ceramic samples of dried clay and mud were prepared, with mud content ranging between 1 and 5 wt %. Ten specimens of each sample were prepared by weighing and mixing both components. An 8 wt % of water was added to the mixture to produce a paste with adequate plasticity to prevent cracks or other defects during the moulding process. Each specimen was obtained by submitting the paste to uniaxial die pressing in a steel matrix. The specimens were then dried in oven at 105 ºC for a 24 h period. Finally, they were sinterized in an oven. The thermal program consisted of a 25 ºC.min⁻¹ heating ramp followed by a 24 h isothermal stage at 950 ºC. The specimens were let to cool inside the oven.

Both clay and industrial mud samples were subjected to chemical, crystalline and thermal characterization. Chemical composition was determined by X-ray fluorescence (WD-XRF) on a Pananalytical (AXIOS model) with Rh tube. The measurement method was semiquantitative flat solid samples with a diameter of 10 mm. The tablet was prepared on a bed of boric acid to obtain a tablet of 40 mm cylindrical. Crystalline phases were determined by X-ray diffraction (XRD) on a Siemens D5000 with graphite monochromator using CuKα radiation. A fresh sample of mud was dried in oven at 105 ºC for a 15 h period. Fresh clay and mud samples and the dry mud specimen were analysed on a Rheometric STA 1500. This is a simultaneous thermal analyzer with the ability to provide simultaneous differential scanning calorimetry (DSC) and thermogravimetric analysis (TG) data. A 20 ºC.min⁻¹ heating rate was applied from room temperature to 900 ºC. Alumina crucibles and a dry air purge at 50 mL.min⁻¹ were used in all the experiments.

Carbonate content in clay and muds was evaluated by the Bernard calcimeter method. This process consists in the measurement of the volume of CO_2 evolved when a finely ground sample is treated with a dilute solution of hydrochloric acid.

The physical and mechanical properties of the final materials were evaluated in order to verify their compliance to building regulations. To this end, linear shrinkage, density, water absorption, sorption and compression strength of all the specimens were measured. The linear shrinkage resulting from the firing process was measured in compliance to the Spanish UNE 67019-86/2R standard. Apparent density is the weight per unit volume of a dry brick, including the voids inherent in the brick. This parameter was measured after a 24 h long drying treatment at 110 ºC (dry) and after the sintering process (fired). Water absorption was determined according to the Spanish UNE 22-182 standard. The specimens were dried in oven at 110 ºC for 24 h and the weight was measured at 1 h intervals until the difference observed between two consecutive measurements was less than 1%. The specimens were then kept at room temperature for 24 h and then slowly introduced into water so that all the specimens were fully submerged. Weight was measured at 24 h intervals until the difference observed between two consecutive measurements was less than 0.1%. The weight of each specimen was weighed after wiping with a damp cloth. The absorbed water is the difference between the wet and dry sample measurements and can be expressed as wt % according to the expression

$$A= [(Ge-Gs)/Gs].100$$

where Gs and Ge represent the weight of the dry and the wet specimen, respectively.

The Spanish standard UNE 67-031 is intended to assess the moisture susceptibility of bricks. Moisture susceptibility represents the potential of a brick to absorb or hold water by capillary rising. This parameter was determined according to the following procedure: the specimens were dried at 110 ºC in an oven until constant weight of each specimen, Pi, was realized. The area, A, of the bottom face of the specimens was measured. Each specimen was placed in a tray with water so that the water level remained constant for one minute at about 3 mm from the bottom of the brick. It was then removed from the tray, wiped with a cloth and weighed. Its weight, Qi, was annotated in grams. The suction, in g.cm⁻² was calculated through the expression

$$S= (Qi-Pi)/A$$

Compressive strength of the fired samples was determined in a compression testing machine as per the Spanish UNE 67-026 standard for marbles and clays. Six specimens of each sample were submitted to normal stress, which was increased at a rate below 20 MPa.s-1 until failure. The contact area was averaged from the measurements in both contact faces of each specimen. Compression stress was obtained by dividing the maximum load by the contact area.

In order to verify whether or not the metals and salts from the industrial muds were ceramized and immobilised into the matrix, a lixiviation test was performed on the fired specimens. Concentrations of minor elements, including Cr, Pb, Zn, As and Cd were previously determined in the mud as per the DIN 38414-S2 standard. The mobility of inorganic analytes present in the samples was determined on the fired

specimens by the Toxicity Characteristic Leaching Procedure (TCLP) [13]. 100 ml of an acetic acid/sodium hydroxide solution with pH=4.93 were incorporated to a 5 g sample of the fired material. Stirring was maintained for 24 h and the solution was then filtered and analysed by Inductively Coupled Plasma Mass Spectroscopy (ICP-MS) on a 7500 AGILENT instrument with Argon plasma ionization and quadrupole detector.

Morphological characterization and energy-dispersive X-ray microanalysis (EDS) were performed on a JSM-5800 JEOL scanning electron microscope, equipped with an ISIS 486 Oxford microanalysis system. Prior to the observations, the samples were Au-metalized through Balzers sputtering.

3. RESULTS AND DISCUSSION

The carbonate contents obtained through the Bernard calcimeter method were 15.08 and 8.53 % for the mud and clay, respectively. Carbonate content is associated to a decrease of the sintering temperature driven by mineralogic transformations in the clay, which favours vitrification and leads to an increase of the glassy phase. It is important to point out that some toxic elements present in the mud could be dissolved and inertized within the glassy phase. These processes will be favoured in the clay by the addition of mud, since the carbonate content in the mud is higher than in the clay. Carbonates also promote whitening of the fired parts and an increase of porosity due to production of CO_2 as a result of carbonate decomposition during the firing process, two well-known effects of these substances.

TABLE 2. MINOR ELEMENT CONTENTS OF THE INDUSTRIAL MUDS, DETERMINED BY ICP-MS.

Element	As	Ba	Cd	Cr	Cu	Ni	Pb	Sr	Zn
Content (ppm)	7.47	69.9	0.66	14.8	5.51	22.7	6.98	186.2	12.52

Table 1 shows the chemical species contents of muds and clay, determined by XRF. The main components observed in the muds were Al_2O_3, CaO, Na_2O, SO_3, F, P_2O_5, Cl and MgO, which is consistent with their origin. As for the clay, its composition is similar to typical industrial clays used in brick manufacturing, with Si, Al, Ca, Fe and K oxides as the main components. There are also important amounts of Ti and Na oxides. Table 2 shows the metal content values obtained from the ICP-MS analysis of the muds.

Figure 1 is a plot of the XRD patterns obtained from the clay. The XRD spectra acquired from the powder and the oriented aggregates show quartz (SiO_2), calcite ($CaCO_3$) and clay minerals including illite ($KAl_2(Si_3Al)O_{10}OH$) as the main crystalline components and, in lower amounts, kaolinite (Aluminium silicate: $Al_4Si_4O_{10}(OH)_8$) and hematites (Fe_2O_3). In the case of the oriented aggregates saturated with glycerol, a small band, which may be an indication of swelling in the 17-20 Å range, can be observed, suggesting the presence of a small amount of smectite. In any case, the clay used in this work is composed of a mixture of illite-clay with high content in quartz and low content in kaolinite, and a marl with possible presence of smectite.

TABLE 1. CHEMICAL CONTENTS OF THE CLAY AND INDUSTRIAL MUDS, DETERMINED BY XRF.

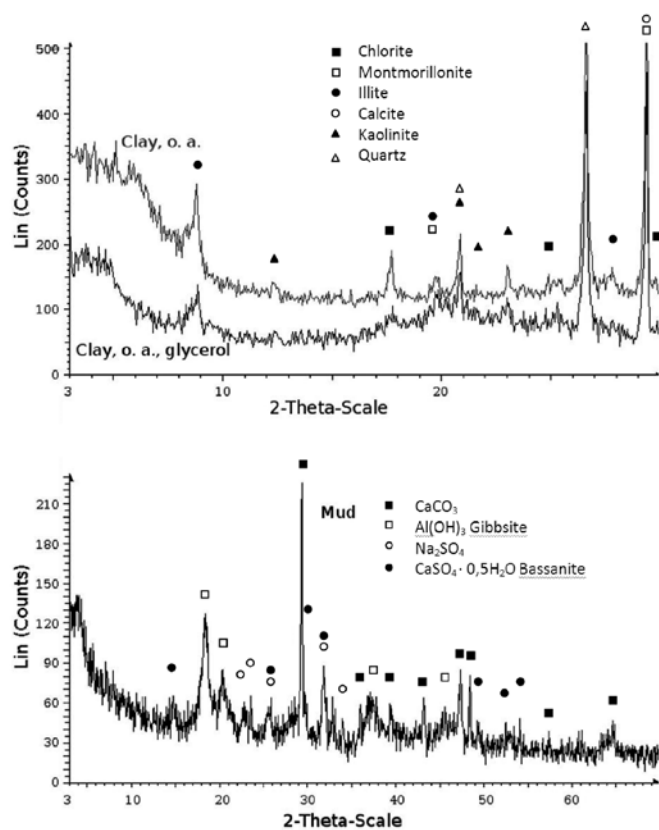| Element oxides	Content (wt %)	
	Industrial muds	Clay
SiO_2	0.52450	55.82
Al_2O_3	43.8754	12.13
Fe_2O_3	0.16689	4.83
MnO	ND	0.03
MgO	0.30993	1.49
CaO	12.1192	9.21
Na_2O	4.62515	0.49
K_2O	0.00795	2.78
TiO_2	0.07947	0.83
P_2O_5	1.35099	0.12
Zr (ppm)	5.64237	279.3
SO_3	11.1496	
F	4.44237	
Cl	0.71523	
Weight loss on ignition at 1000 ºC	20.53	10.55

Figure 1. XRD patterns obtained from the clay by the oriented aggregates method, with and without glycerol saturation, and from the industrial mud powder.

Figure 1 also shows the XRD patterns obtained from the industrial muds, and indicates gibbsite and calcite as the major components. A lower content of calcium fluoride, gypsum and cryolite can also be observed. Bassanite, sodium sulphate, calcium phosphate and halite are also present, although in small amounts.

The DSC, TG and TG derivative (DTG) traces obtained from the fresh clay sample are shown on Figure 2. The most significant weight loss processes associated to brick manufacturing are free water evaporation and carbonate decomposition. Water evaporation mainly occurs at temperatures below 100 ºC, although it extends up to 150 ºC, overlapping with a small dehydration process at about 107 ºC. In both cases, simultaneous DTG and endothermic DSC peaks are observed. The loss of weight associated with these processes is 1.7 %.

There are other minor DSC and DTG events that overlap strongly in the range from 150 to 600 ºC. These events are probably related to dehydration processes. Particularly,

a small endothermic peak, which can be attributed to dehydroxylation of the laminar silicates present in the sample, can be observed at 570 ºC. The overall weight loss measured in this range was about 1.8 %. Calcium carbonate decomposition takes place in the range between 600 and 800 ºC [14], as evidenced by a DTG and an endothermic DSC peaks. These peaks are strongly asymmetric, indicating that the rate of the process increases with temperature until the carbonates are exhausted. It is important to point out that carbonate decomposition evolves CO_2. Since the samples will be fired at 900 ºC, decomposition of carbonates is expected, and therefore, the higher the carbonate content, the higher the porosity of the fired samples. The weight loss measured in this range was 9.1 %, which would correspond to a calcium carbonate content of 21 % on a dry basis, considering a moisture content of about 1.7 %. Nevertheless, Table 1 shows that the CaO content determined by XRF in a dry sample is 9.2 %, which corresponds to a 16.4 % of $CaCO_3$. The difference, 4.6 %, is due to other overlapping processes. Other compounds may be originated from the reaction of the products resulting from dehydroxylation of silicates with alkaline and alkaline earth oxides originated in other decomposition processes. It is possible that some of these compounds and other carbonates present in lower concentrations in the sample decompose in the same temperature range as calcium carbonate. Figure 2 also shows the DSC, TG and DTG plots obtained from a fresh and a dried mud samples. In both cases, a continuous weight loss was observed along the entire experiment, which indicates overlapping processes. This adds difficulty to knowing the amount of sample involved in each single process. The accumulated weight losses observed at 900 ºC were 64.71 and 27.64 % for the fresh and dry samples, respectively. The difference, 37.07 %, can be attributed to the free water content. The important weight loss observed, even in the dry mud sample, suggests that its incorporation into a clay matrix will produce voids or shrinkage, or both, during the firing. In the first sample case, simultaneous DTG and endothermic DSC peaks are observed at 124 and 291 ºC. Although both processes overlap, the first one can be attributed to free water evaporation and the second to calcium sulphate dehydration. In the case of the dry sample, a higher sample weight was used in order to enhance sensitivity. The plotting scale was enlarged in order to show more clearly the small changes taking place during the progression of the experiment. In addition, a fitting of the DTG curve to a mixture of derivative logistic functions was performed with the Fityk software [15] in order to separate overlapping processes. The model can be written as
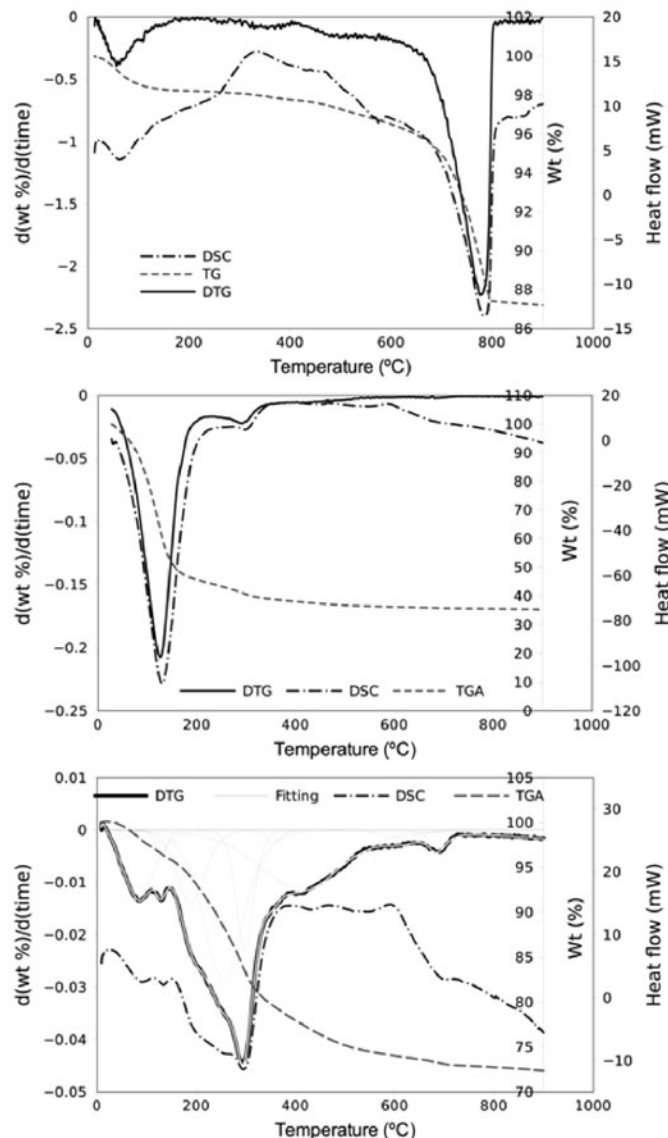

Figure 2. DSC, TG and DTG traces obtained from a fresh clay sample (a), a fresh mud sample (b) and a dry mud sample (c).

$$Y(t) = \sum_{i=1}^{k} \left[\frac{w_i \exp\left(\dfrac{c_i + t}{d_i}\right)}{d_i\left(\exp\left(\dfrac{c_i}{d_i}\right) + \exp\left(\dfrac{t}{d_i}\right)\right)^2} \right]$$

where w_i represents the amount of weight loss involved in each single process, c_i is the point on the time axis, t, where each component is centered and d_i is related to the width of the peaks. The criterion for optimizing the fitting consisted in minimizing the weighted sum of squared residuals (WSSR).

An optimal fitting was found with a WSSR value of 8.31211e-05. Both the fitting and the single components are plotted on Figure 2. Table 3 shows the parameter values of the fitting and the temperature values corresponding to the central points. Prior experience with the TG instrument indicates that temperature readings below 80 ºC are not accurate since the instrument was designed to work at a higher temperature range. In any case, a very small gain of weight was observed at room temperature, which indicates gas absorption by the sample. Although a dry air purge was used, wet air was present inside the TG furnace at the beginning of the experiment since it had to be opened for sample positioning. The weight increase observed is 0.22 % and is probably due to water and N_2 absorption. The same gases were released at about 50 ºC. Small but well defined simultaneous DTG and endothermic DSC peaks are observed at 83 and 131 ºC, which corresponds to the logistic components (LC), obtained by the fitting, centered at 84.7 and 128.9 ºC, respectively. The first one, representing a 3.3 % weight loss, can be attributed to sodium carbonate dehydration [16, 17, 18]. The broad endotherm with peak at 291 ºC presents two shoulders on the left side corresponding to the TG LC centered at 188.5 and 254.8 ºC, as it can be observed on the same plot. The 128 and 188 ºC LC account for almost a 3.5 % and can be easily assigned to gypsum and bassanite dehydration, which were identified by XRD [19, 20]. The 254 ºC component, accounting for an 8.7 % of the weight loss, might have been contributed by evolved water from particle surfaces during the transition from gibbsite to boehmite since it was reported to take place in a range around 247 ºC [21,22]. According to Table 1, small amounts of magnesium carbonate hydrates may exist. In that case, dehydration of these hydrates would also contribute, although in small amount, to this LC [23]. The component at

297.3 ºC, representing a 3.0 %, should be assigned to gibbsite dehydroxylation [24, 21]. As it was described for ungrounded samples [24], a further gradual weight loss could be completed by 700 ºC overlapping with other processes. Another small LC appears at 352.5 ºC, which can be explained as constitutional water release from the phosphate content of the sample. It accounts for only a 0.29 % weight loss and, although there is not any evident simultaneous endotherm, a change of slope can be observed on the DSC curve indicating a potential hidden endotherm. It was reported that monobasic sodium phosphate produces three weight losses at 122, 210 and 343 ºC [25]. The last one, corresponding to the pyrophosphate-metaphosphate transformation, can be attributed to the 352.5 ºC LC. The processes at 122 and 210 ºC would be masked by the more important contribution of the previously described events. An important 7.0 % weight loss LC is centered at 410.1 ºC. It spans both sides along a wide range of temperature, which indicates that it probably accounts for more than one single process. Although it was also reported that hydrated calcium phosphate becomes anhydrous at 294°C and it turns into calcium pyrophosphate ($Ca_2P_2O_7$) at 554 ºC [26], the TG plot on that report shows that maximum weight loss rate is reached in the 200-250 ºC and 400-475 ºC ranges, although a continuous weight loss is observed up to 500 ºC. This is consistent with the fact that the central part of the 410 ºC LC is mainly due to pyrophosphate formation and that the low temperature half of the peak includes phosphate

TABLE 3. PARAMETER VALUES AND TEMPERATURE VALUES CORRESPONDING TO THE CENTRAL POINTS OBTAINED BY THE FITTING OF THE DRY MUD DTG CURVE TO A MIXTURE OF DERIVATIVE LOGISTIC FUNCTIONS.

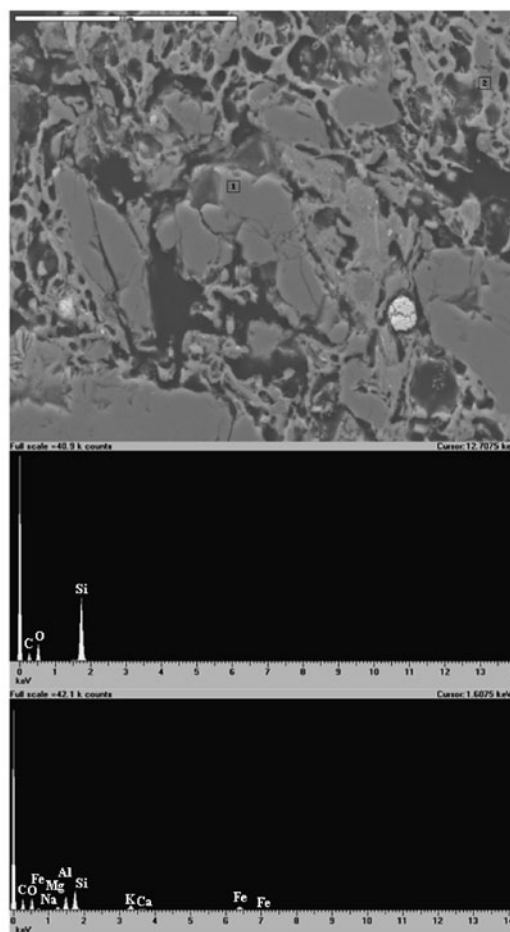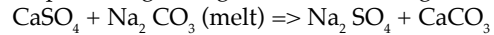| Component	w (%)	c (s)	d	Temperature (°C)	DSC	Main contribution events
1	-0.220335	82.0654	37.95	about 20ºC		N_2 and H_2O absorption
2	0.225949	296.088	35.54	about 50ºC		N_2 and H_2O release
3	3.31773	428.644	64.53	84.7	Endo peak	Sodium carbonate dehydration
4	0.466071	568.751	21.9678	128.9	Endo peak	Gypsum and bassanite dehydration
5	3.01319	742.414	53.6285	188.5	Endo shoulder	Gypsum and bassanite dehydration
6	8,74968	930.71	75.9116	254.8	Endo shoulder	Gibbsite dehydroxylation
7	2.96947	1052.88	32.3244	297.3	Endo peak	Gibbsite dehydroxylation
8	0,285186	1201.15	29.0577	352.5		Pyrophosphate-metaphosphate transformation
9	7.02341	1359.87	154.91	410.1		Pyrophosphate formation, phosphate dehydration
10	0.436152	1942.78	70.5404	613.4		Magnesium carbonate decomposition
11	0.450565	2156.37	35.0725	685.4	Endo peak	Calcium carbonate desomposition
12	14.4703	4197.16	516.219	1373.4 (extrapolated)	Endo	Reaction of remnant sodium carbonate with calcium sulphate

Figure 3. SEM micrograph obtained from a 5 % mud sample and the XRF spectra obtained at the indicated locations.

dehydration. This LC probably also includes part of the gibbsyte dehydroxylation, which was reported to expand up to 700 ºC [24] and magnesium carbonate decarbonation [23]. Another LC, accounting for only a 0.44 % of the weight sample, is located at 613.4 ºC. It is somewhat spreaded along the temperature axis and can also be attributed to magnesium carbonate decarbonation [27]. It was reported that calcium carbonate decomposition takes place between 680 and 776°C [28], and, in the case of some red muds, between 560 and 720°C [29]. In this work, calcium carbonate decarbonation is represented by a well shaped LC at 685.4 ºC, which is accompanied by a simultaneous endotherm. The DTG plot shows a slight increase of the weight loss rate at the end of the experiment. The 12th LC was included to subtract this weight loss process from the other components, but their parameter values cannot be taken into account because the main part of this fictive LC falls out of the experimental range. In any case, the later weight loss observed can be due to the reaction of

remnant sodium carbonate with calcium sulphate originating sodium sulphate and calcium carbonate, which immediately decomposes originating the observed weight loss [30]:

$$CaSO_4 + Na_2CO_3 \text{ (melt)} => Na_2SO_4 + CaCO_3$$

The morphological study of the fired samples was based on the SEM observations. Figure 3 shows the image obtained from a 5 % mud sample. The apparent predominance of a vitreous phase can be attributed to clay being the main component, as well as to the role of CaO and Al_2O_3 generated from the mud in promoting glass formation. An homogeneous distribution of the mud in the ceramic matrix can be observed in Figure 3. The results of the microanalysis performed at the locations labelled as 1 and 2 on the picture are also shown. Location 1 corresponds to a clay rich region. Muds, in turn, predominate at location 2, where Fe, Al, Mg, Ca and K were identified. Figure 4 shows a micrograph of a 4 % mud sample. Three points were labelled indicating the locations where microanalysis was performed.
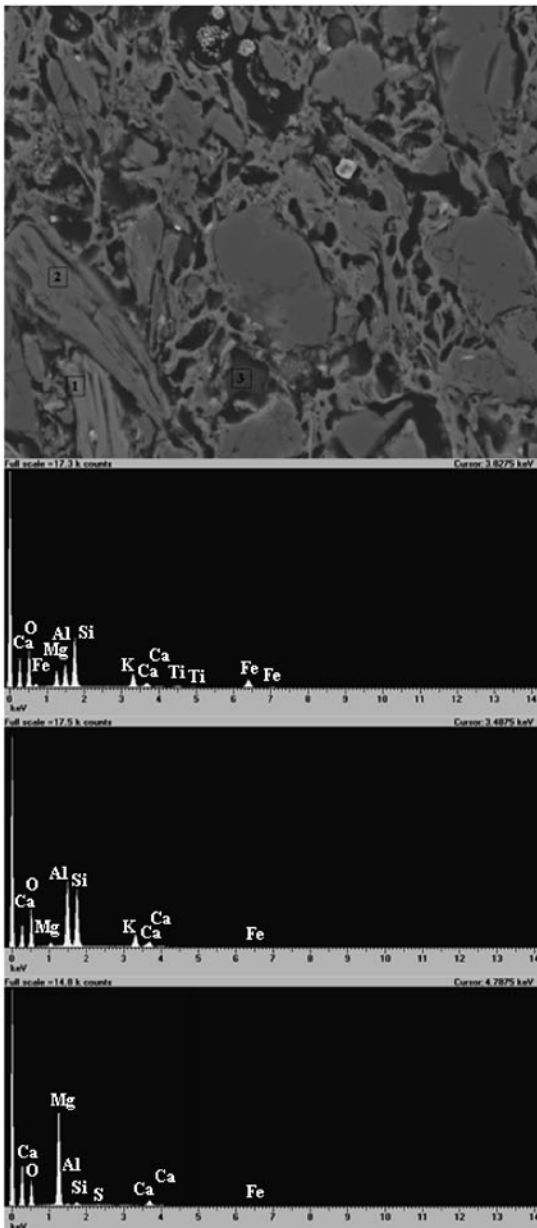

Figure 4. SEM micrograph obtained from a 4 % mud sample and the XRF spectra obtained at the indicated locations.
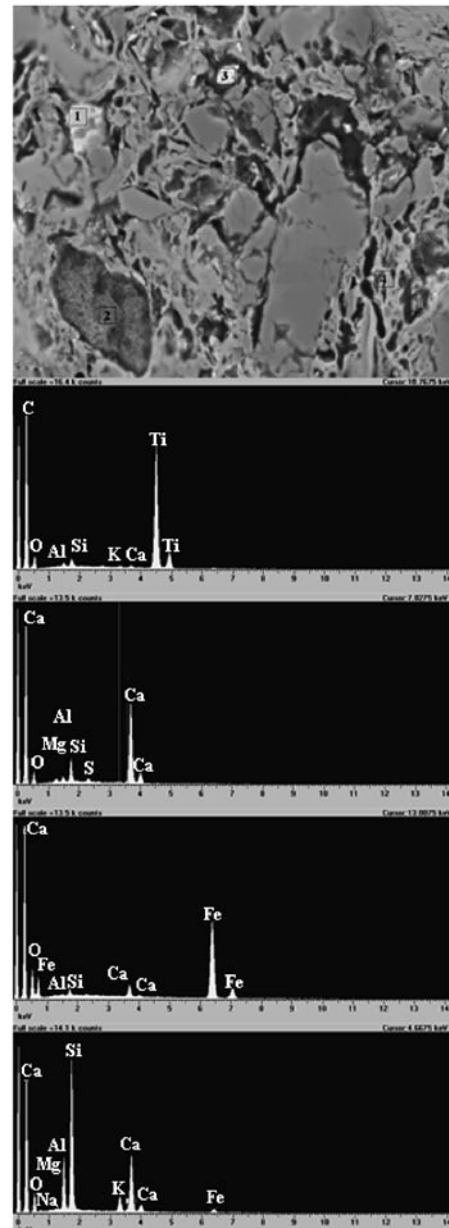

Figure 5. SEM micrograph obtained from a 2 % mud sample and the XRF spectra obtained at the indicated locations.
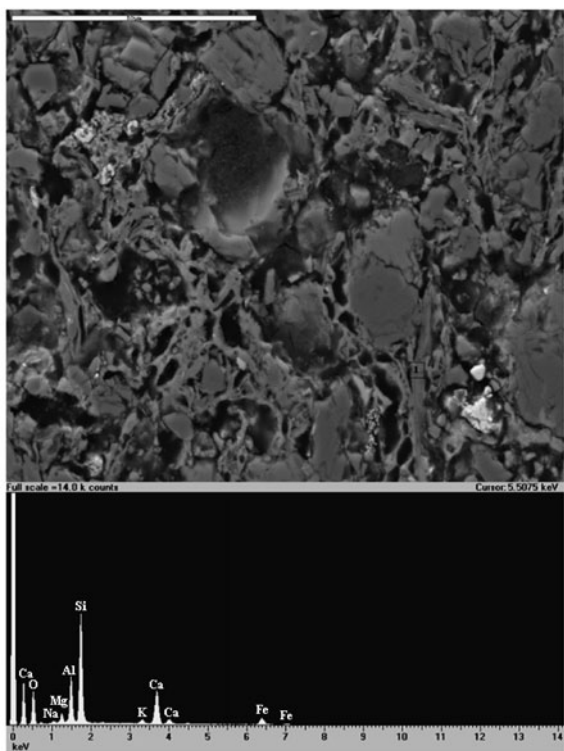
Figure 6. SEM micrograph obtained from a 1 % mud sample and the XRF spectra obtained at the indicated location.

TABLE 4. ICP-MS (PPB) RESULTS OBTAINED IN THE LIXIVIATION TEST OF THE SAMPLES WITH DIFFERENT MUD CONTENTS.

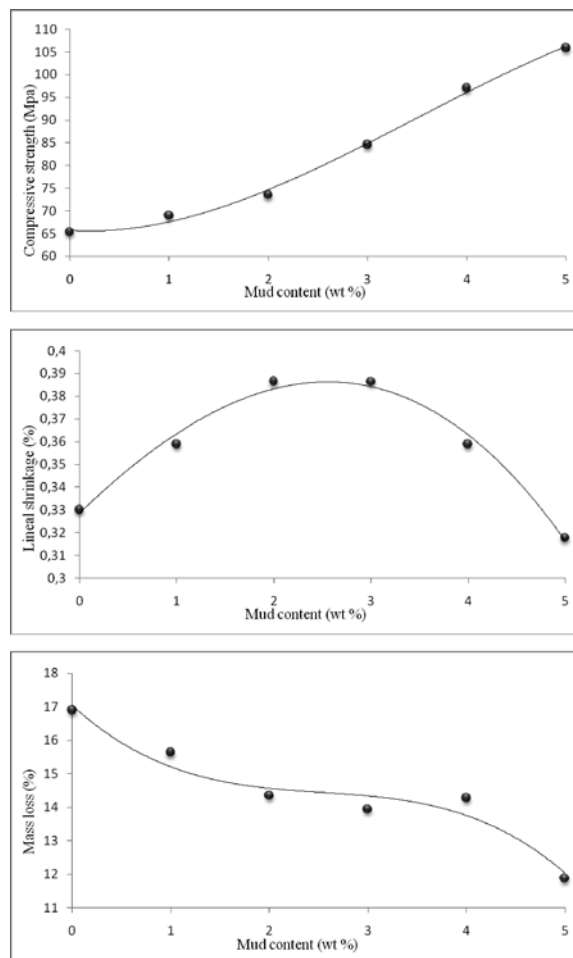|	Concentration (ppb)					
	Mud content in the sample (wt %)					
Element	1	2	3	4	5	EPA regulated TCLP limit
Al	0.76	0.49	0.6	0.75	1.89	
V	408.02	258.97	297.72	300.42	217.32	
Cr	448.4	625.6	624.4	755.5	1024.7	5000
Fe	1652.8	1851.3	1843.8	2012.3	1807.8	
Co	0.33	0.28	0.96	1.74	1.81	
Ni	1.55	1.81	1.64	2.32	3.28	5000
Cu	11.61	12.10	11.11	11.43	12.39	10000-2000
Ga	0.84	1.38	1.17	1.19	2.75	
As	15.38	1.08	2.04	1.05	1.81	5000
Se	1.85	1.24	1.66	1.78	2.92	1000
Rb	71.6	79.04	67.97	71.23	102.29	
Sr	1452.81	1871.81	1698.81	1906.81	1729.81	
Ag	0.22	0.22	0.22	0.22	0.30	5000
Cs	1.69	1.46	1.16	1.15	3.59	
Ba	55.67	94.40	85.08	78.57	85.52	100000
Tl	0.18	0.10	0.18	0.39	2.4	

Figure 7. Compressive strength, linear shrinkage and weight loss at the sinterization obtained from samples with different mud content.
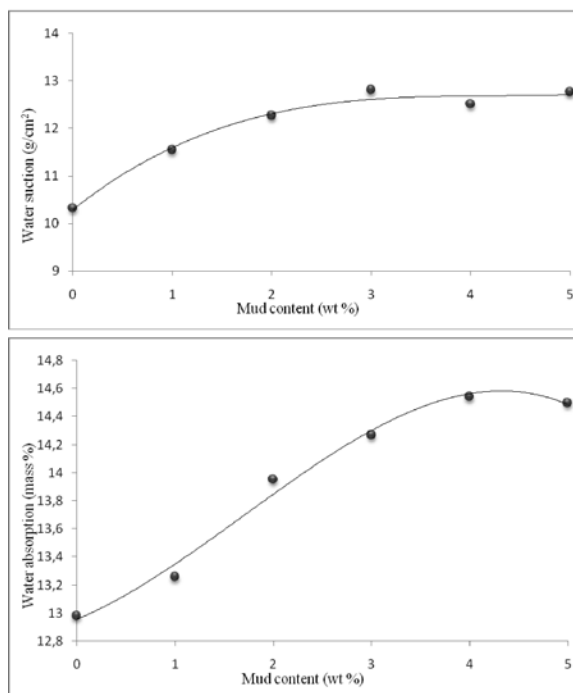

Figure 8. Water suction and absorption observed in samples with different mud contents.

The morphological study can be seeing on the SEM observations (fig. 3-6).

Table 4 shows the results of the lixiviation tests, along with the limits established by the U. S. Environmental Protection Agency (EPA). It is worth mentioning that all the concentrations determined in the samples are well below the regulated limits.

Compressive stress is a critical parameter for structural applications of ceramics in building. The UNE-EN 772-1 Spanish standard establishes a minimum value of 10 MPa for bricks. Figure 8 plots the compression and shrinkage results obtained from the samples with different mud contents. It can be observed that compressive strength increases, almost linearly, with the mud content. An increment of 35 % is observed in the 5% mud sample (100 MPa), with respect to the clay-only sample (65 MPa). This increment is due to the glassy phase generated by the CaO and Al_2O_3 present in the industrial muds. It can be also observed that the effect of the mud on the contraction is almost negligible. Although very slight, a stabilizing effect of the mud is observed, so the weight loss at the sinterization stage decreases when the mud content increases.

Water suction and absorption results are shown in Figure 9. Both values increase with mud content, although not seriously. It indicates a higher hydration susceptibility of the oxides originated from the mud.

4. CONCLUSIONS

The use of up to 5 % of anodization aluminium waste muds as raw material for brick manufacturing was possible. The bricks obtained presented improved mechanical properties. Water suction and absorption were not seriously affected. The obtained bricks comply with the toxicity regulations for recycling waste materials. A whitening effect of the muds was observed, which broadens the range of application of these bricks.

Apart from the environmental interest, the incorporation of these muds as raw material can lead to important reductions in manufacturing costs.

REFERENCES

1. E. González, J. L. Asenjo, A. Baena, J. Dufour, A. La Iglesia, A. Hernández, N Cornejo, E. Ruiz Ayúcar, E. García, N. Ayala, F. García Carcedo, F. Delmás, J. R. Mayarl, Application of anodising muds in several industrial fields. Proceedings of the Rewas'99: Global Symposium on Recycling, Waste Treatment and Clean Technology, Vol. 1, 481-490, San Sebastian, Spain (1999)
2. J. Dufour, M. V. González, A. La Iglesia, Optimization model for the recovery of residual effluents of anodising industry. In: Gaballah I, Hager J, Solozabal R. editors. Proceedings of the Rewas'99: Global Symposium on Recycling, Waste Treatment and Clean Technology, Vol. 1, 597-606, San Sebastian, Spain (1999)
3. E. Álvarez Ayuso, Approaches for the treatment of waste streams of the aluminium anodising industry. J. Hazard. Mater., 164, 2-3, 409-414 (2009)
4. R. R. Menezes, G. A. Neves, H. C. Ferreira, O estado da arte sobre o uso de residuos como matérias-primas cerâmicas alternativas. Revista Brasileira de Engenharia Agrícola e Ambiental, 6, 2, 303-313 (2002)
5. E. Rambaldi, A. Tucci, L. Espósito, D. Naldi. Utilización de residuos OVH en la industria cerámica. Bol. Soc. Esp. Ceram. V.49, 4, 259-264 (2010)
6. D.M. Couto, J.A. Labrincha, R. F. Silva, L. Guise, F. Castro, Attempts of incorporation of metal plating sludges in ceramic products. Ind. Ceram., 21, 4, 163-168 (2001)
7. D. A. Pereira, J. B. Aguiar, F. P. Castro, M.F. Almeida, J. A. Labrincha, Mechanical behavior of Portland cement mortars with incorporation of Al-rich salt slags. Cem. Concr. Res., 30, 7, 1131-1138 (2000)
8. J. A. Pérez, R. Terradas, M. R. Manent, M. Sejas, S. Martinez, Inertization of industrial wastes in ceramic materials. Ind. Ceram. 16, 1, 7-10 (1996)
9. M. J. Ribeiro, D. U. Tulyaganov, J. M. Ferreira, J. A. Labrincha, Recycling of Al-rich industrial sludge in refractory ceramic pressed bodies. Ceram. Int., 28, 3, 319-326 (2002)
10. D. M. Couto, A. Ringuedé, R. F. Silva, J.A. Labrincha, C. M. S. Rodrigues, Metallurgical sludge in clay-based fired materials, Am. Ceram. Soc. Bull., 82, 12, 9101-9103 (2003)
11. M. Dondi, M. Marsigli, B. Fabbri, Recycling of industrial and urban wastes in brick production-a review (part 1). Tile Brick Int., 13, 3, 218-225 (1997)
12. M. B. Almendro Candel, M. M. Jordán, M. Romero, J. M. Rincón, Aplicación del residuo lodo de depuradora en la fabricación de productos de arcilla cocida. Residuos, 15, 82, 148-151 (2005)
13. Toxicity Characteristic Leaching Procedure. TCLP; Method 1311-1. In: Environmental Protection Agency SW-846 report 1992. Downloaded from Environmental Health & Safety Online. Http://www.ehso.com.
14. D. Dollimore, P. Tong, K. S. Alexander, The kinetic interpretation of the decomposition of calcium carbonate by use of relationships other than the Arrhenius equation. Thermochim. Acta, 13, 27, 282-283 (1996)
15. Fityk ver. 0.8.2 for Linux. Software 2007, Fityk online homepage: http://www.unipress.waw.pl/fityk/.
16. R. Jordán, T. Faria, G. Rodríguez, G. César-Díaz, M. E. Zayas, Estudio de las transformaciones térmicas en la elaboración de un vidrio sódico-cálcico para envases con zeolita natural cubana. Ing. Cienc., 3, 6, 91-105 (2007)
17. C. Bayuadri, Stability of sodium sulphate dicarbonate ($2Na_2CO_3Na_2SO_4$) crystals. MS degree Thesis. School of chemical and biomolecular engineering, Georgia Institute of Technology, (2006)
18. P. K. Heda, D. Dollimore, K. S. Alexander, D. Chen, E. Law, P. Bicknell, A method of assessing solid state reactivity illustrated by thermal decomposition experiments on sodium bicarbonate. Thermochim. Acta, 255, 255-272 (1995)
19. R. A. Kuntze, Differential thermal analysis of calcium sulphate dihydrate. Nature, 193, 772-773 (1962)
20. W. E. P. Fleck, M. H. Jones, R. A. Kuntze, H. G. McAdie, The differential thermal analysis of natural and synthetic hydrates of calcium sulphate. Can. J. Chem., 38, 6, 936-943 (1960)
21. M. R. Hill, T. J. Bastow, S. Celotto, A. J. Hill, Integrated study of the calcination cycle from gibbsite to corundum. Chem. Mater., 19, 11, 2877-2883 (2007)
22. D. Fonseca, F. Barba, P. Callejas, P. Recio. Comportamiento térmico de los minerales no metálicos de Cayo Guan, Cuba. Bol. Soc. Esp.Ceram. V.48, 3, 171-178 (2009)
23. A. Botha, C. A. Strydom, DTA and FT-IR analysis of the rehydration of basic magnesium carbonate. J. Therm. Anal. Calorim., 71, 3, 987-995 (2003)
24. K. J. D. MacKenzie, J. Temuujin, K. Okada, Thermal decomposition of mechanically activated gibbsite. Thermochim. Acta, 327, 103-108 (1999)
25. H. J. De Jager, L. C. Prinsloo, The dehydration of phosphates monitored by DSC/TGA and in situ Raman spectroscopy. Thermochim. Acta, 376, 187-196 (2001)
26. G. Madhurambal, R. Subha, S.C. Mojumdar, Crystallization and thermal characterization of calcium hydrogen phosphate dihydrate crystals. J. Therm. Anal. Calorim., 96, 1, 73-76 (2009)
27. Z. Hao, J. Pan, F. Du. Synthesis of basic magnesium carbonate microrods with a surface of "house of cards" structure. Mater. Lett., 63, 12, 985-988 (2009)
28. A. Alp, M. S. Gora, The influence of soda additive on the thermal properties of red mud. J Therm. Anal. Calorim., 73, 1, 201-207 (2003)
29. Y. Liu, C. Lin, Y. Wu, Characterization of red mud derived from a combined Bayer Process and bauxite calcination method. J. Hazard. Mater., 146, 1-2, 255-261 (2007)
30. J. Wang, Y. Wu, E. J. Anthony, Reactions of solid $CaSO_4$ and Na_2CO_3 and formation of sodium carbonate sulphate double salts. Thermochim. Acta, 459, 121-124 (2007)